AQUA
Water Infrastructure, Ecosystems and Society

IWA PUBLISHING

AQUA — Water Infrastructure, Ecosystems and Society Vol 73 No 4, 771 doi: 10.2166/aqua.2024.300

Green synthesis of iron nanoparticles from the baru (*Dipteryx alata*) endocarp extract for the efficient removal of rhodamine B and caffeine from water through the heterogeneous Fenton process

Cassiano Ricardo Reinehr Corrêa[a], Adriano Buzutti de Siqueira[b], Paulo Renato Matos Lopes[c], Jéssica Aparecida Ribeiro Ambrosio[d], Andreza Ribeiro Simioni[d], Leonardo Gomes de Vasconcelos[a,b] and Eduardo Beraldo de Morais[a,e,*]

[a] Postgraduate Program in Water Resources, Federal University of Mato Grosso, Cuiabá, MT, Brazil
[b] Department of Chemistry, Federal University of Mato Grosso, Cuiabá, MT, Brazil
[c] Department of Plant Production, College of Agricultural and Technological Sciences, São Paulo State University, Dracena, SP, Brazil
[d] Research and Development Institute, Vale do Paraíba University, São José dos Campos, SP, Brazil
[e] Department of Sanitary and Environmental Engineering, Federal University of Mato Grosso, Cuiabá, MT, Brazil
*Corresponding author. E-mail: beraldo_morais@yahoo.com.br

EBd, 0000-0002-8505-4133

ABSTRACT

This study presents the first-time synthesis of iron nanoparticles (FeNPs) using an aqueous extract from the baru fruit endocarp (*Dipteryx alata*). Characterization through scanning electron microscopy and dynamic light scattering revealed spherical shapes with an average diameter of 419.2 nm. Fourier transform infrared spectroscopy identified phytochemicals from the baru fruit extract, acting as both reducing and stabilizing agents. X-ray diffraction confirmed the amorphous nature of the FeNPs. The Fenton-like catalytic efficiency of FeNPs was investigated for degrading rhodamine B (RhB) and caffeine. The impact of crucial parameters such as pH, H_2O_2 dosage, nanoparticles concentration, and temperature on the degradation process was assessed. At pH 3.0, with 1.0 g L^{-1} of FeNPs, 1% H_2O_2, and 45 °C, RhB and caffeine degradation reached 99.14 and 92.01%, respectively. The catalytic reaction kinetics followed a pseudo-first-order model for caffeine and a pseudo-second-order model for RhB. Phytotoxicity studies on *Cucumis sativus* confirmed the non-toxic nature of the degraded products of RhB and caffeine. These findings highlight the potential of FeNPs synthesized from the baru endocarp extract as a catalyst for removing organic pollutants, suggesting promising applications in environmental remediation and related fields.

Key words: Fenton-like catalysis, green chemistry, iron nanoparticles, metallic nanoparticles, plant extract

HIGHLIGHTS

- Green iron nanoparticles were successfully synthesized using an extract derived from the endocarp of the baru fruit (*Dipteryx alata*).
- The catalytic potential was validated against rhodamine B (RhB) and caffeine.
- Phytotoxicity investigations involving *Cucumis sativus* affirmed the non-toxic characteristics of the degraded products of RhB and caffeine.

GRAPHICAL ABSTRACT

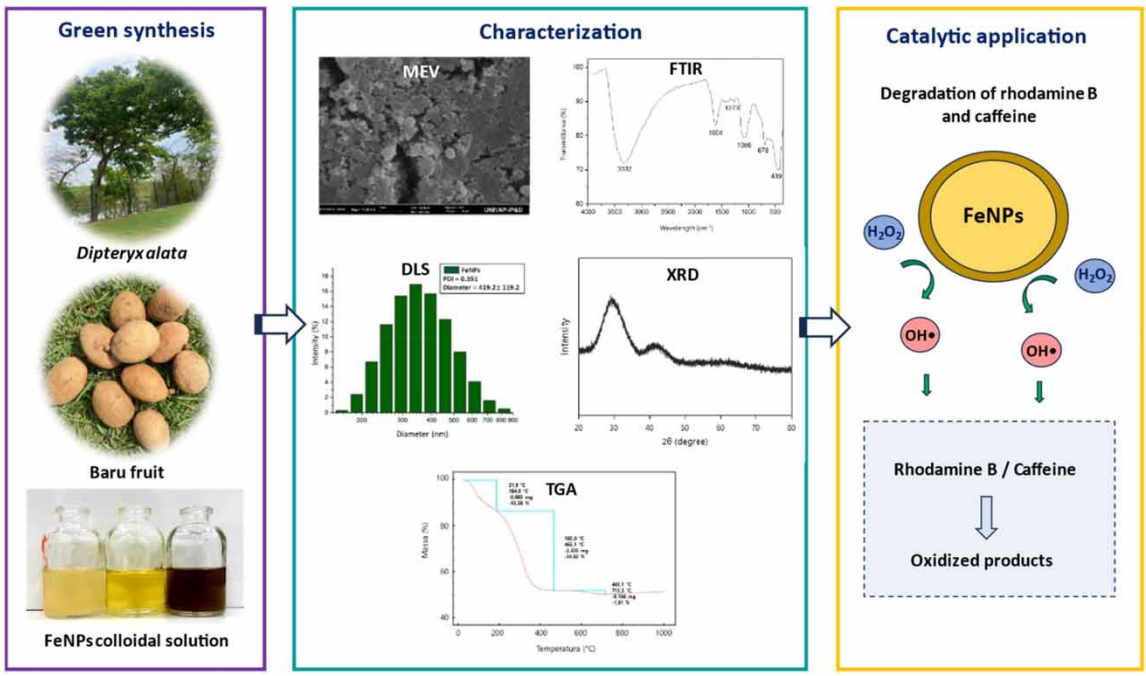

INTRODUCTION

Nanotechnology has witnessed remarkable advancements in recent decades, leading to the exploration of various nanomaterials, including metallic nanoparticles (MNPs). MNPs possess exceptional properties that make them highly desirable for numerous applications across diverse fields such as medicine, microbiology, agriculture, materials science, energy, and the environment (Madubuonu *et al.* 2019; Selvaraj *et al.* 2022; Suppiah *et al.* 2023). These properties include a high surface area per unit volume, remarkable mechanical and thermal strength, distinct optical and magnetic characteristics, as well as antimicrobial and catalytic properties (Fahmy *et al.* 2018; Priya *et al.* 2021; Narayanan *et al.* 2021). As a result, MNPs have garnered significant attention and research interest.

However, traditional methods of synthesizing MNPs using chemical and physical approaches have certain limitations. These methods, including coprecipitation, hydrothermal synthesis, sol–gel processes, and microemulsion, often involve the use of toxic-stabilizing and -dispersing agents that can be harmful to living organisms and the environment (Selvaraj *et al.* 2022). Additionally, they require substantial amounts of energy, making the synthesis process costly (Anchan *et al.* 2019). Hence, there is a need for sustainable and cost-effective alternatives that overcome these drawbacks.

One promising approach is the utilization of biological systems for MNP synthesis. Among the various biological sources, plant tissues have gained attention due to their abundance and accessibility (Jadoun *et al.* 2021). Extracts derived from different plant species contain phytochemicals that act as reducing and stabilizing agents for the nanoparticles (Madubuonu *et al.* 2019). This biofabrication method offers numerous advantages over traditional techniques. Firstly, plant extracts provide a sustainable and eco-friendly alternative, as they eliminate the need for toxic chemicals and reduce environmental impacts (Suppiah *et al.* 2023). Additionally, plant extracts are cost-effective and readily available, making them accessible for large-scale production. Moreover, the biofabrication process using plant extracts is relatively simple, requiring less energy and time compared to complex chemical and physical methods (Demirezen *et al.* 2019; Jadoun *et al.* 2021).

Among the metals used for MNP synthesis, iron nanoparticles (FeNPs) have emerged as particularly important due to their wide-ranging applications. FeNPs exhibit antioxidant and antimicrobial properties, making them useful in medicine and microbiology (Bharathi *et al.* 2020; Suppiah *et al.* 2023). In agriculture, FeNPs promote plant growth and serve as a micronutrient fertilizer (Alabdallah *et al.* 2021; Haydar *et al.* 2022). They also serve as effective adsorbents for various pollutants and can be utilized in advanced oxidative processes (AOPs) for water treatment (Guo *et al.* 2020; Pai *et al.* 2021; Khoshkalam

et al. 2023). In recent studies, different plant tissues have been explored for the synthesis of FeNPs, including leaves, roots, and fruits of various plant species (Demirezen *et al.* 2019; Ting & Chin 2020; Pai *et al.* 2021; Ningthoujam *et al.* 2023). However, the synthesis of FeNPs using the endocarp of the baru fruit (EB) (*Dipteryx alata*) has not been investigated before. The baru fruit, a tree species from the Fabaceae family, is native to Brazil and widely distributed in the Cerrado biome (Niedack *et al.* 2021). While the mesocarp and nuts of the fruit are used for food purposes, the endocarp remains an underutilized by-product (Rambo *et al.* 2021). Exploring the potential of baru fruit endocarp for FeNPs synthesis could provide new opportunities for sustainable and value-added utilization of this biomass.

Organic dyes play a crucial role in the manufacturing of paints, plastics, leather, rubber, and cosmetics, contributing to the development of products that are vivid and aesthetically pleasing (Briton *et al.* 2019). However, the discharge of these dyes as waste in industrial effluents has emerged as a significant environmental challenge. Annually, approximately 700,000 tons of organic dyes are released into water bodies, impacting sunlight penetration, inhibiting photosynthesis, and adversely affecting the aquatic life (Jain *et al.* 2021). Pharmaceutical compounds constitute another group of potential contaminants in aquatic ecosystems. The improper disposal of unused medications and the incomplete removal of pharmaceutical residues during wastewater treatment contribute to the presence of these substances in water bodies (Talib & Randhir 2017). These pharmaceutical compounds can adversely affect aquatic ecosystems and pose potential risks to human health. The continuous exposure of aquatic organisms to low concentrations of pharmaceuticals has been linked to various negative effects, including altered behavior, reproductive disruptions, and developmental abnormalities (Valdez-Carrillo *et al.* 2020; Jijie *et al.* 2021; Ríos *et al.* 2022). Moreover, the potential for these substances to accumulate in the food chain raises concerns about their impact on human health (Osuoha *et al.* 2023).

Rhodamine B (RhB) and caffeine are two common organic pollutants in water and wastewater, which represent the class of dyes and pharmaceuticals, respectively. RhB is a xanthene dye that is widely utilized in the textile, paint, leather, and paper industries (Wang *et al.* 2019). Despite its widespread application, experimental studies have confirmed its carcinogenicity, genotoxicity, and chronic toxicity (Golin *et al.* 2022). Caffeine is an alkaloid belonging to the class of methylxanthines, and it is found in over 60 plant species. It holds significant pharmaceutical relevance, as it is used to reduce fatigue, increase alertness, and enhance the effectiveness of analgesics used to treat colds and headaches (Bachmann *et al.* 2021). Caffeine is also a compound commonly found in beverages and foods such as teas, coffees, chocolates, and energy drinks (Korekar *et al.* 2020). Numerous studies have identified the presence of caffeine in wastewater, surface water, and groundwater (Li *et al.* 2020; Rani 2022), with anthropogenic contamination being the primary source of this pollution. Despite the impacts of the presence of caffeine in water bodies still being unknown, adverse effects such as enzyme alterations, lipid peroxidation, reduction in energy reserves, and oxidative stress have already been demonstrated in mollusk and fish (Cruz *et al.* 2016; Muñoz-Peñuela *et al.* 2021).

The negative environmental consequences of water pollution caused by dyes and pharmaceuticals emphasize the need for sustainable practices and innovative solutions in industrial processes (Ismail *et al.* 2022; Aneke & Adu 2023). AOPs emerge as a viable alternative for eliminating organic contaminants from water. These processes involve the generation of highly reactive species, such as hydroxyl radicals (·OH) or sulfate radicals ($\cdot SO_4^-$), which, as potent oxidizing agents, can lead to the breakdown of organic pollutants (Guo *et al.* 2020). Among AOPs, the homogeneous Fenton reaction is a traditional method that involves the generation of hydroxyl radicals through the catalytic decomposition of H_2O_2 by iron salts (Fe^{2+}, Fe^{3+}) (Briton *et al.* 2019). However, there are some drawbacks that can limit its application. It is highly pH-dependent, requiring acidic conditions for optimal performance (typically pH 2.5–4), which may restrict its use in certain environments (Wu *et al.* 2015). The generation of large amounts of iron sludge as a byproduct, inefficient utilization of H_2O_2, and the inability to recover the catalyst also pose challenges, necessitating careful control and management (Wang *et al.* 2019). On the other hand, the heterogeneous Fenton process using a solid catalyst offers an alternative to address these drawbacks. Among these solid catalysts, green FeNPs have been successfully employed for removing bisphenol A (Guo *et al.* 2020), lindane (Ningthoujam *et al.* 2023), monochlorobenzene (Kuang *et al.* 2013), malachite green (Ting & Chin 2020), and methylene blue (Madubuonu *et al.* 2019) from water and wastewater.

In this study, we present the first-time synthesis of FeNPs using an aqueous extract obtained from the baru fruit endocarp. The FeNPs were characterized using various techniques, including Fourier transform infrared spectroscopy (FTIR), scanning electron microscopy (SEM), dynamic light scattering (DLS), X-ray diffraction (XRD), and thermogravimetric analysis (TGA). Furthermore, FeNPs were employed as catalysts in a heterogeneous Fenton-like system for the removal of RhB and caffeine from an aqueous solution, with an investigation into the impact of initial solution pH, FeNPs and hydrogen peroxide dosages,

and temperature on the removal process. Additionally, we assessed the phytotoxicity of the degradation products of RhB and caffeine to confirm their non-toxic nature.

MATERIALS AND METHODS

Chemicals

All chemical reagents were of analytical grade. Ferrous sulfate heptahydrate ($FeSO_4{\cdot}7H_2O$), RhB ($C_{28}H_{31}ClN_2O_3$), and hydrogen peroxide (H_2O_2, 29%) were purchased from Synth, Brazil. Caffeine ($C_8H_{10}N_4O_2$) was obtained from Sigma-Aldrich. All solutions were prepared using distilled water.

Preparation of an aqueous extract from the baru fruit endocarp

The EB was collected in the state of Mato Grosso, which is located in the Midwest region of Brazil. The EB was washed abundantly with distilled water, air-dried, and ground to a fine powder using a steel-knife electrical mill (Figure 1(a)). To prepare the aqueous EB extract, 10 g of dry EB were stirred with 1,000 mL of distilled water for 1 h at 80 °C. Subsequently, the extract was vacuum-filtered, and the filtrate was stored at 4 °C for further studies.

Synthesis of FeNPs

The synthesis of FeNPs was adapted from Bharathi *et al.* (2020). A solution of ferrous sulfate (0.1 M) was mixed with the EB extract at a 1:1 (v/v) ratio and stirred at 80 °C for 2 h. The change in color from light yellow to brownish-black indicated the formation of FeNPs (Figure 1(b)). The synthesized nanoparticles were collected by centrifugation (8,000 rpm, 15 min), washed twice with distilled water to remove ions and residues from the EB extract, and dried in an oven at 80 °C for 24 h.

Characterization of FeNPs

The FeNPs were characterized using techniques such as FTIR, SEM, DLS, XRD, and TGA. For FTIR analysis, a Shimadzu IRAffinity-1 spectrometer was utilized. Samples were prepared as KBr discs, and the spectrum was recorded in the range of 4,000–400 cm^{-1}. SEM images were captured using a Zeiss EVO-MA10 instrument with an acceleration voltage of 20 kV. Particle size and frequency distribution were measured by the laser light scattering technique using DLS (Malvern Zetasizer Nano ZS, Malvern, UK). XRD analysis was conducted using a Bruker D8 Advance diffractometer with Cu Kα radiation, operating at a voltage of 40 kV and a current of 40 mA. TGA data were obtained using a Shimadzu DTG-60H thermogravimetric analyzer. The TGA curve was obtained using a synthetic air atmosphere and a heating rate of 20 °C min^{-1}, ranging from room temperature to 1,000 °C.

Fenton-like catalytic activity of FeNPs

Fenton-like catalytic assays were conducted in 150 mL Erlenmeyer flasks containing an aqueous solution of RhB or caffeine at a concentration of 20 mg L^{-1}. The flasks were agitated at 150 rpm using a thermostatic rotary shaker. The study investigated the effects of initial solution pH (2.0, 3.0, 4.0, 5.0, 6.0, and 7.0), FeNPs dosage (0.2, 0.4, 0.6, 0.8, and 1.0 g L^{-1}), H_2O_2 dosage (0.25, 0.5, 0.75, 1.0, and 1.5%), and temperature (25, 35, and 45 °C) on degradation to determine optimal reaction conditions. Control assays using only FeNPs or H_2O_2 were compared to those involving both FeNPs and H_2O_2 to

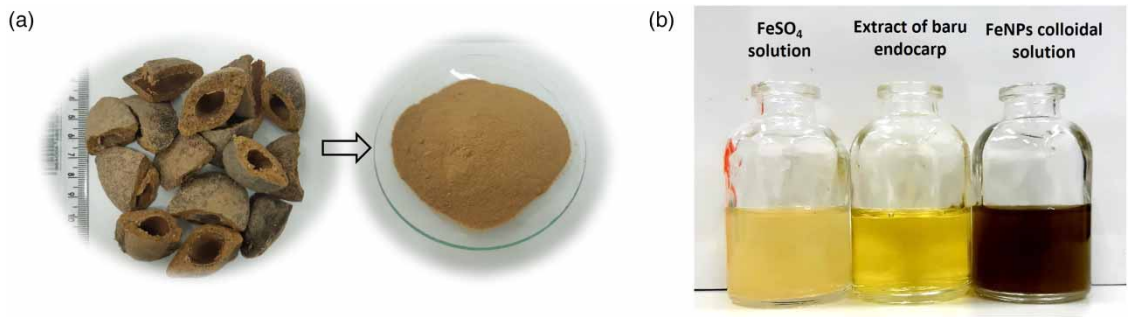

Figure 1 | (a) Baru fruit endocarp used for extract preparation. (b) Ferrous sulfate solution, baru fruit endocarp extract, and FeNP colloidal solution.

understand the degradation process of RhB and caffeine. At regular intervals, samples were collected from the reaction mixture and centrifuged at 8,000 rpm for 15 min. The concentrations of RhB and caffeine were determined using standard plots recorded at $\lambda = 543$ nm (RhB) and $\lambda = 237$ nm (caffeine) in a UV–Visible spectrophotometer (Hach DR6000). Subsequently, the removal efficiency of RhB and caffeine was calculated using Equation (1):

$$R(\%) = \frac{C_0 - C_t}{C_t} \times 100 \quad (1)$$

where C_0 is the initial concentration of RhB or caffeine (mg L^{-1}) and C_t is the concentration at time t (min).

Kinetic studies of the degradation of RhB and caffeine were also conducted using both pseudo-first- and pseudo-second-order kinetic models, as described by Equations (2) and (3) (Guo *et al.* 2020):

$$-\ln\frac{C_t}{C_0} = k_1 t \quad (2)$$

$$\ln\left(\frac{1}{C_t} - \frac{1}{C_0}\right) = k_2 t \quad (3)$$

where k_1 and k_2 represent the pseudo-first-order rate constant (min^{-1}) and pseudo-second-rate constant (L mg^{-1} min^{-1}).

Phytotoxicity of degradation products of RhB and caffeine

In the process of degrading organic contaminants, it is crucial that the resulting degradation products demonstrate non-toxic properties. Therefore, toxicity bioassays were carried out using *Cucumis sativus* seeds (cucumber) to evaluate the potential toxic effects of RhB and caffeine degradation products. Ten seeds were placed on 90 mm diameter Petri dishes containing filter paper moistened with 5 mL of the solution to be tested. The plates were then incubated at 23 °C for 5 days in the dark, with distilled water used as the negative control. Tests were conducted in triplicate. Subsequently, the germinated seeds, along with the lengths of the radicle and hypocotyl, were recorded for comparison with the control.

RESULTS AND DISCUSSION

Characterization of FeNPs

During the synthesis of FeNPs, a dark brown-colored solution was formed when the $FeSO_4$ solution and the EB extract were mixed (Figure 1(b)). The change in color is the primary indicator of FeNPs synthesis, and it occurs due to the reduction of ferrous ions by phytochemicals present in the extract (Anchan *et al.* 2019). The FeNPs were characterized using various techniques. The FTIR technique allowed us to identify main functional groups present on the surface of the FeNPs (Figure 2). The broad and strong band at 3,332 cm^{-1} is attributed to the stretching vibrations of –OH groups in saccharides and polyphenols (Madubuonu *et al.* 2019). The band at 1,606 cm^{-1} corresponds to the stretching vibrations of the C = C aromatic ring (Barizão *et al.* 2020). The bands at 1,273 and 1,056 cm^{-1} correspond to the stretching vibrations of C–O bonds in alcohols and phenols (Rocker *et al.* 2019). The bands at 678 and 439 cm^{-1} are associated with the bending vibrations of Fe–O groups (Anchan *et al.* 2019), suggesting the successful synthesis of FeNPs. These functional groups clearly indicate the presence of EB extract phytochemicals on the surface of the nanoparticles which act as capping and stabilizing agents.

The morphology of FeNPs was monitored through SEM images, confirming the formation of particles with a spherical shape and a certain degree of agglomeration (Figure 3(a)). This agglomeration, which was also reported in the studies conducted by Pai *et al.* (2021) and Khoshkalam *et al.* (2023), is a result of the interaction between the organic molecules present on the surface of the nanoparticles. The size distribution of the FeNPs obtained by DLS analysis showed that the particles had an average diameter of 419.2 ± 119.2 nm with a polydispersity index (PDI) of 0.351 (Figure 3(b)). Similarly, FeNPs synthesized from the extract of *Solanum lycopersicum* leaves showed an average size of 483 nm and a PDI of 0.31 (Bharathi *et al.* 2020), while FeNPs synthesized using the extract of *Ficus carica* fruit showed an average size of 475 nm (Demirezen *et al.* 2019).

Figure 4 shows the X-ray diffractogram obtained for the FeNPs. No defined diffraction peaks were observed, suggesting that the nanoparticles have an amorphous nature. The broadband observed at $2\theta = 30°$ can be attributed to the presence of organic matter from the EB extract adsorbed on the nanoparticles (Xiao *et al.* 2016). The XRD results are consistent with

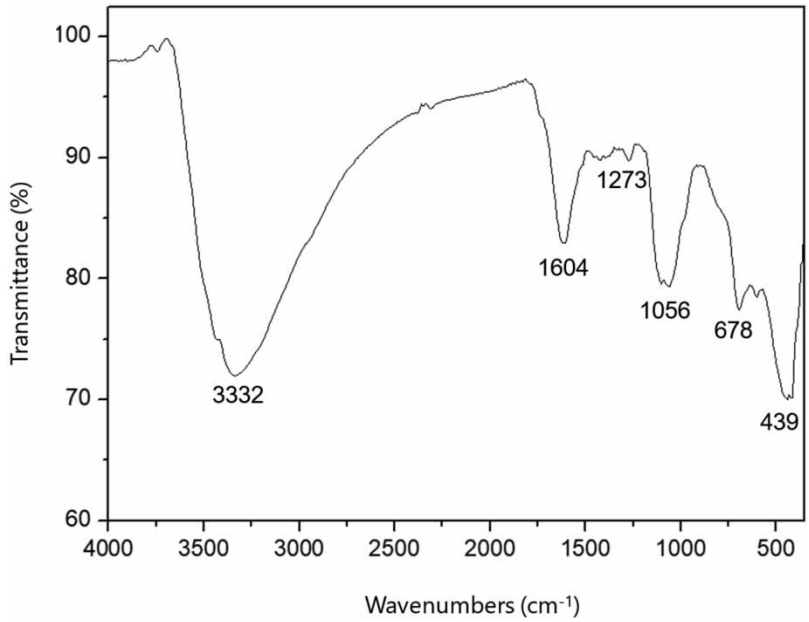

Figure 2 | FTIR spectrum for green FeNPs.

the electron microscopy results discussed earlier. Other studies that synthesized FeNPs from plant extracts have also reported similar diffraction patterns to those observed in the present study (Irshad *et al.* 2017; Lourenço *et al.* 2019).

The mass loss profile of the FeNPs as a function of temperature is presented in Figure 5. A loss of 13.28% of mass was observed between 31 and 184 °C, resulting from the evaporation of water present in the sample, as well as the evaporation of volatile compounds (Anchan *et al.* 2019). Between temperatures of 185 and 465 °C, the mass loss was higher (34.62%) and is related to the thermodegradation of biomolecules from the EB extract present on the surface of the FeNPs. A reduction of 1.61% in mass was still observed between temperatures of 465 and 713 °C, due to the thermodegradation of aromatic structures present in the biomolecules, which are more resistant to degradation (Rolim *et al.* 2019). No significant changes in mass were observed between 713 and 1,000 °C. Therefore, it is possible to affirm that the phytochemical compounds along with the adsorbed water represent approximately 50% of the mass of the FeNPs.

Heterogeneous Fenton-like oxidation of RhB and caffeine by FeNPs

Effect of pH

Given that the pH of the solution affects both the activity of the oxidant and the stability of hydrogen peroxide, the influence of pH (2.0–7.0) on the degradation of RhB and caffeine was monitored (Figure 6). The removal of these compounds was also evaluated in solutions containing only H_2O_2 or FeNPs. The degradation of RhB by Fenton-like oxidation reached 97.27% at pH 3.0 and then decreased as the pH increased, reaching 87.81% at pH 7.0 (Figure 6(a)). Caffeine degradation followed the same pattern, with the maximum degradation reaching 86.96% at pH 3.0 and decreasing to 41.53% at pH 7.0 (Figure 6(b)). This can be attributed to the fact that under acidic conditions, the surface of FeNPs is corroded, and iron oxides are leached, generating Fe^{2+} ions, which, in turn, produces hydroxyl radicals (Kuang *et al.* 2013). This process is described by Equations (4) and (5) (Guo *et al.* 2020):

$$Fe^0\ (FeNPs) + H_2O_2 + 2H^+ \rightarrow Fe^{2+} + 2H_2O \quad (4)$$

$$Fe^{2+} + H_2O_2 \rightarrow Fe^{3+} + \cdot OH + OH^- \quad (5)$$

The decrease in the degradation of RhB and caffeine observed at higher pH values is attributed to the reduction in the oxidation potential of ·OH and the precipitation of iron oxides and hydroxides, leading to a decrease in the concentration

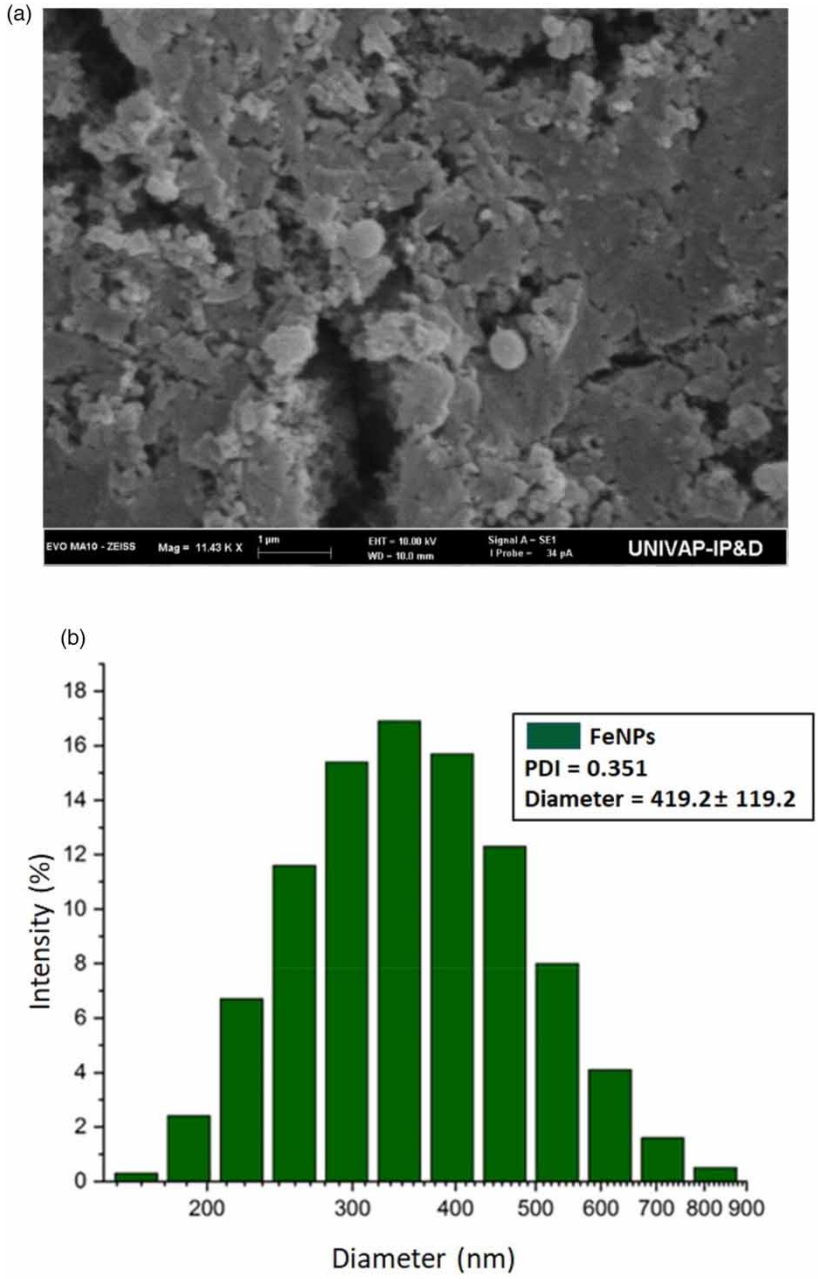

Figure 3 | SEM image (a) and (b) DLS size distribution of the green FeNPs.

of Fe^{2+} and Fe^{3+} ions in the solution (Wu *et al.* 2015). Furthermore, the degradation of RhB and caffeine declined to 89.03 and 59.59%, respectively, when the pH was reduced to 2.0. This decline is associated with hydrogen ions acting as scavengers for hydroxyl radicals (Babuponnusami & Muthukumar 2012) and the solvation of hydrogen peroxide, resulting in the formation of a stable oxonium ion $[H_3O_2]^+$ in the presence of highly concentrated H^+ ions (Rusevova *et al.* 2012). The identified optimum pH value (pH = 3.0) aligns with other studies that employed FeNPs as catalysts to degrade various pollutants, such as phenol (Babuponnusami & Muthukumar (2012)), monochlorobenzene (Kuang *et al.* 2013), bisphenol A (Guo *et al.* 2020), and methyl orange (Yuan *et al.* 2020).

In Figures 6(a) and 6(b), it is also possible to observe that in the system containing only H_2O_2, the degradation of RhB and caffeine remained minimal across all evaluated pH levels (1.94–4.77 and 1.95–3.88%, respectively). In contrast, in the system

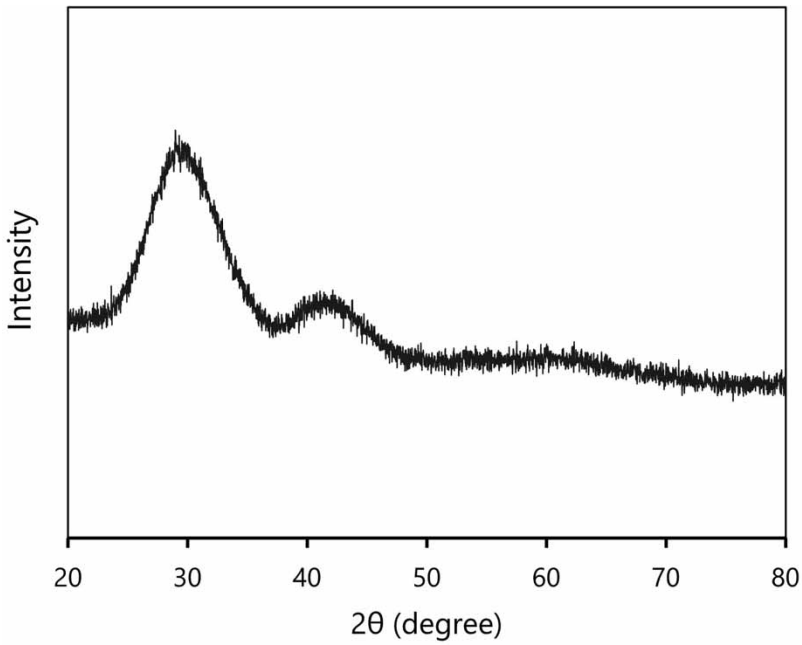

Figure 4 | XRD analysis for green FeNPs.

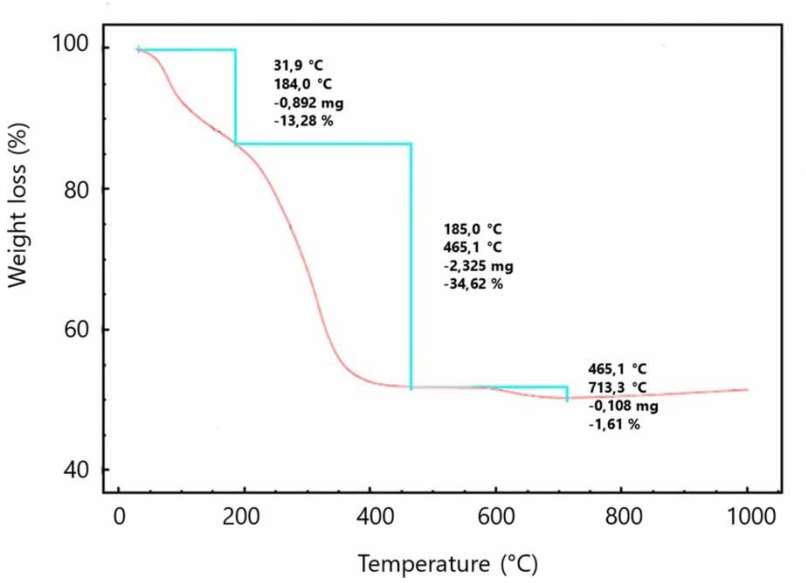

Figure 5 | Mass loss profile of green FeNPs as a function of temperature.

containing only FeNPs, RhB removal ranged from 28.71 to 36.14%, and caffeine removal ranged from 16.46 to 16.20%. These results can likely be attributed to the adsorption of these compounds by the nanoparticles. This affirms the excellent catalytic activity of FeNPs synthesized from the baru fruit endocarp extract in the Fenton oxidation of RhB and caffeine.

Despite the decrease in RhB and caffeine degradation at higher pH values, the efficacy of FeNP-mediated degradation remains satisfactory in the pH range of 4–6, particularly for RhB. This is advantageous for the practical application of the heterogeneous Fenton process in wastewater treatment. In contrast, the homogeneous Fenton process typically exhibits high efficiency only at pH values around 3.0. Dhahir *et al.* (2014) achieved close to 100% degradation rates for RhB in a

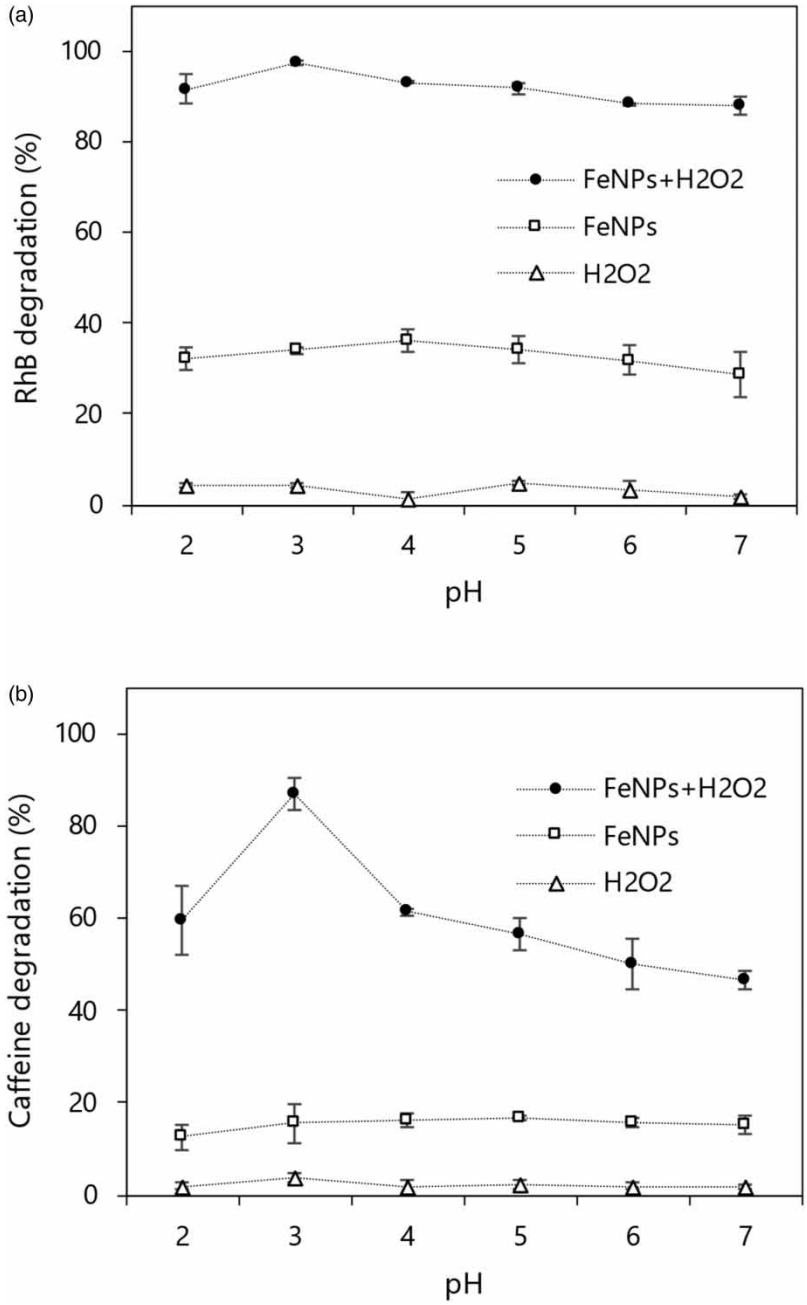

Figure 6 | Effect of initial solution pH on the oxidative degradation efficiency of RhB (a) and caffeine (b) using FeNPs as a catalyst (experimental conditions: H_2O_2 dosage = 1%, FeNP dosage = 1.0 g L^{-1}, temperature = 25 °C, reaction time = 180 min).

$UV/H_2O_2/Fe^{2+}$ system at pH 2.0 and 3.0; however, at pH 6.0, the rates declined to around 20%. Similarly, Oliveira *et al.* (2015) reported caffeine degradation rates of up to 95% using the homogeneous Fenton reaction at pH 3.0, but degradation sharply declined at pH values exceeding 4.0.

Effect of FeNP dosage

The impact of FeNPs dosage on the degradation of RhB and caffeine was examined within the range of 0.20–1.0 g L^{-1} at an initial pH value of 3.0, as illustrated in Figure 7. With an increase in dosage from 0.2 to 1.0 g L^{-1}, RhB degradation increased from 54.03 to 97.27%, and caffeine degradation increased from 37.13 to 86.96%. This escalation is likely attributed to the amplification of active sites for H_2O_2 decomposition, leading to the generation of more ·OH and consequently enhancing

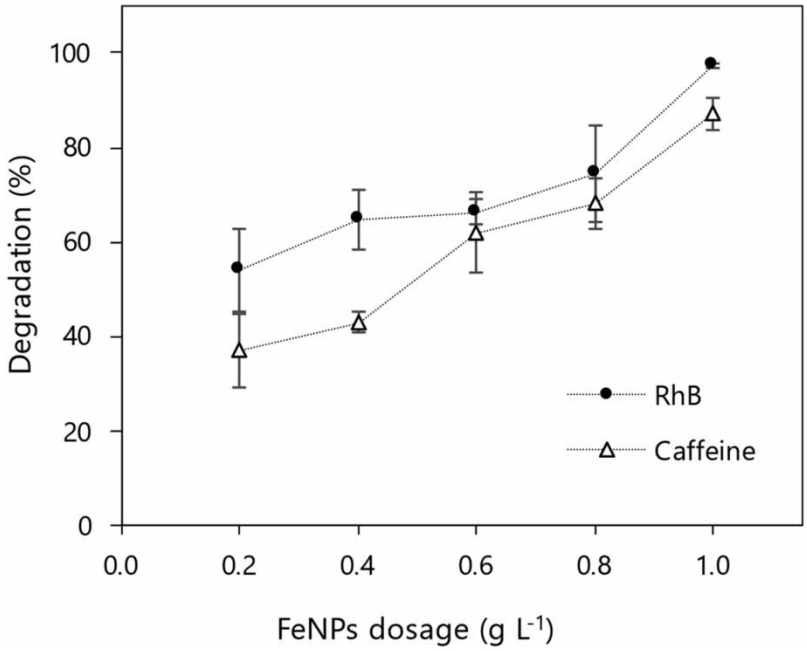

Figure 7 | Effect of FeNP dosage on the oxidative degradation efficiency of RhB and caffeine (experimental conditions: pH = 3.0, H_2O_2 dosage = 1%, temperature = 25 °C, reaction time = 180 min).

degradation efficiency. Similar findings were reported by Kuang *et al.* (2013), Briton *et al.* (2019), and Guo *et al.* (2020). However, Wu *et al.* (2015) and Hassan *et al.* (2020) highlighted a limit beyond which an increase in FeNP dosage does not further enhance pollutant degradation. Beyond this threshold, degradation diminishes due to nanoparticle agglomeration and hydroxyl radical scavenging by an excess of Fe^{2+} in the solution (Equation (6)):

$$Fe^{2+} \cdot OH \rightarrow Fe^{3+} + OH^{-} \tag{6}$$

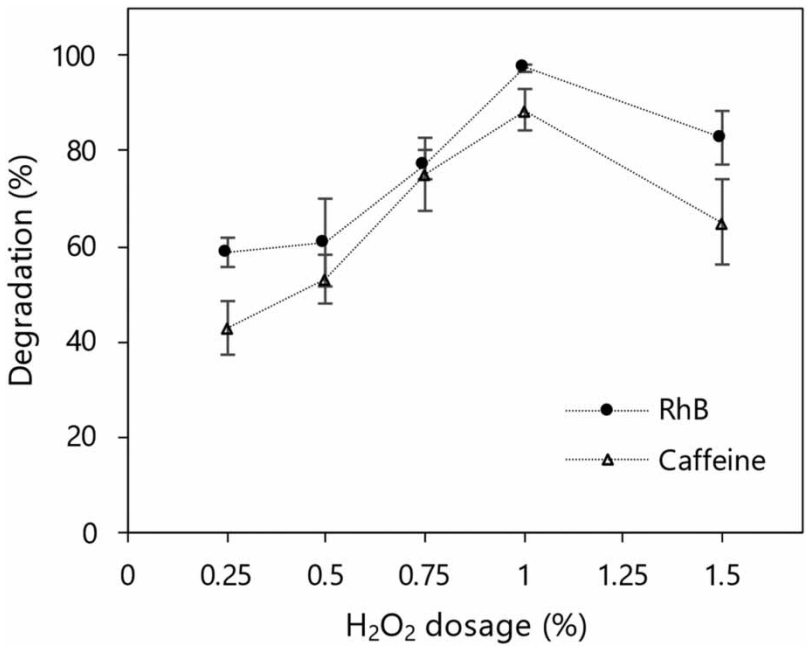

Figure 8 | Effect of H_2O_2 dosage on the oxidative degradation efficiency of RhB and caffeine (experimental conditions: pH = 3.0, FeNP dosage = 1.0 g L^{-1}, temperature = 25 °C, reaction time = 180 min).

Effect of H_2O_2 dosage

The dosage of H_2O_2 in the Fenton-like oxidation process is another crucial factor impacting the degradation of organic compounds, as it directly influences the production of hydroxyl radicals. The influence of H_2O_2 dosage on the degradation of RhB and caffeine is presented in Figure 8. The degradation of both organic substances increased with the rise in H_2O_2 dosage from 0.25 to 1.0%: from 58.91 to 97.27% for RhB and 43.10 to 88.45% for caffeine. However, a further increase in H_2O_2 dosage to 1.5% did not lead to enhanced degradation; instead, a reduction was observed (82.64% for RhB and 65.36% for caffeine). This decrease is attributed to the recombination of hydroxyl radicals with excess H_2O_2, forming hydroperoxyl radicals ($HO_2\cdot$). As $HO_2\cdot$ is less reactive than ·OH radicals, a reduction in the degradation of RhB and caffeine occurs (Hassan *et al.* 2020).

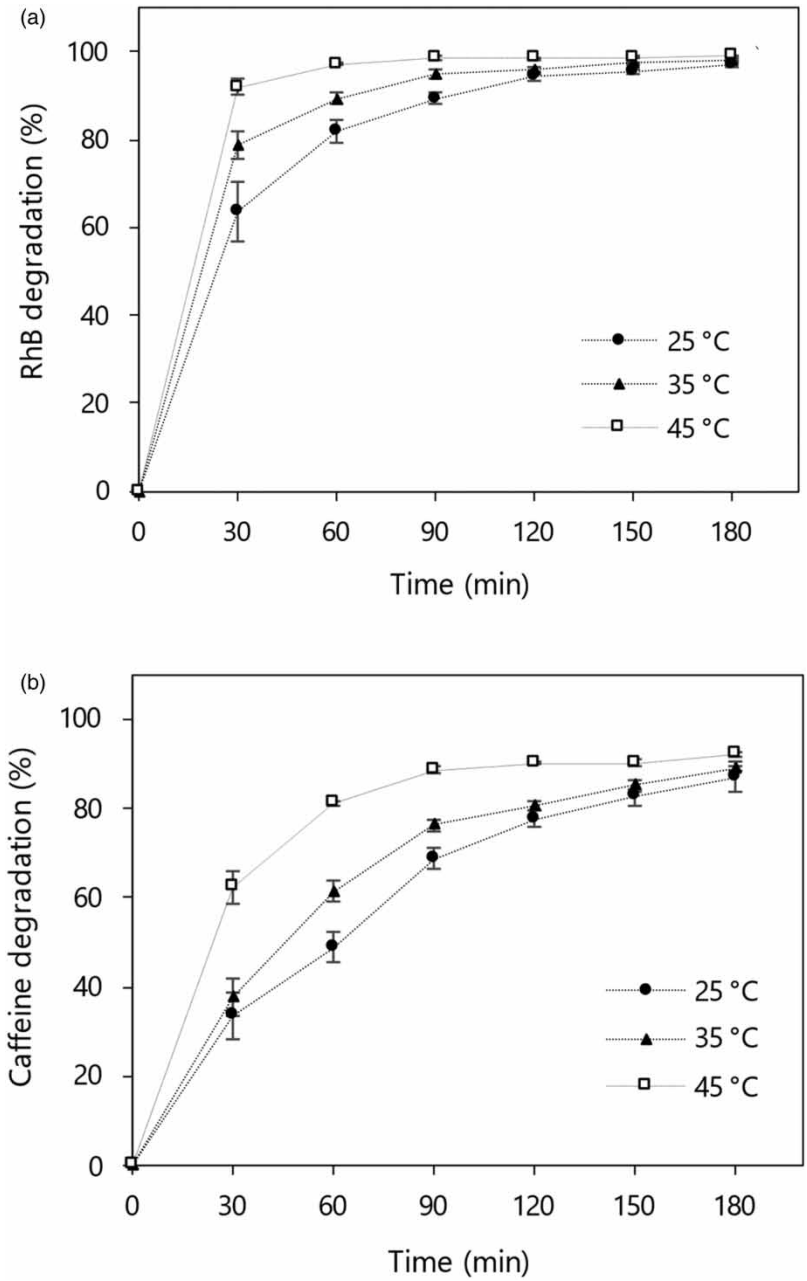

Figure 9 | Effect of reaction time on the degradation of RhB (a) and caffeine (b) at different temperatures (experimental conditions: pH = 3.0, H_2O_2 dosage = 1%, FeNP dosage = 1.0 g L^{-1}).

This process can be elucidated by Equation (7):

$$H_2O_2 + \cdot OH \rightarrow H_2O + HO_2\cdot \quad (7)$$

Effect of temperature and oxidative kinetics

As shown in Figure 9, the impact of temperature on the degradation of RhB and caffeine was investigated at temperatures of 25, 35, and 45 °C. It became evident that temperature has a positive effect on the degradation of both organic compounds. At the 30-min mark from the start of the reaction, the degradation of RhB and caffeine increased from 63.47 to 91.80% and from 33.54 to 62.20%, respectively, as the temperature rose from 25 to 45 °C. Subsequently, the degradation rate gradually

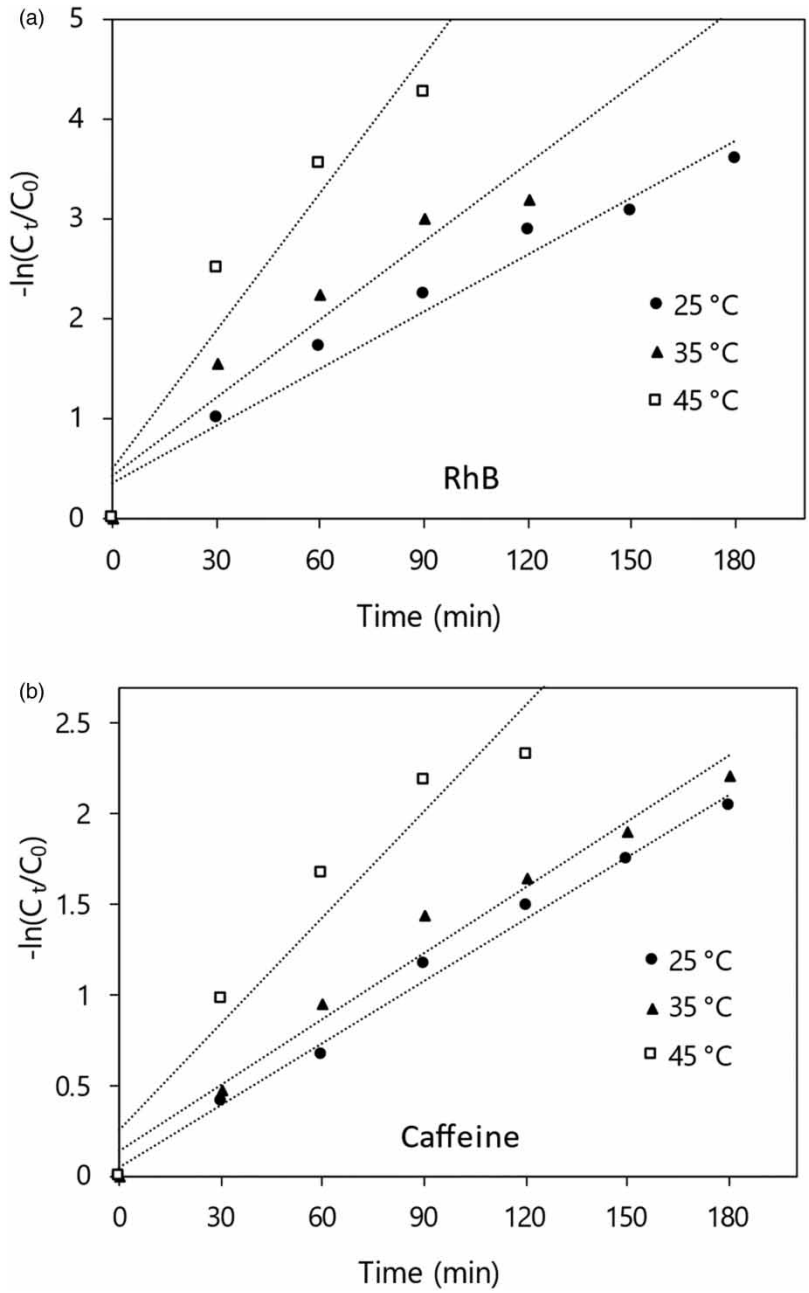

Figure 10 | Pseudo-first-order kinetic model for RhB (a) and caffeine (b) degradation.

decreased. After 180 min, RhB and caffeine degradation reached 97.27 and 86.96%, respectively, at 25 °C, and 99.13 and 92.01%, respectively, at 45 °C. The positive effect of temperature on degradation can be explained by: (1) the accelerated catalysis of H_2O_2 at a higher temperature, leading to a heightened generation of hydroxyl radicals (·OH); (2) increased collision frequency between FeNPs and reactants, ultimately enhancing the efficiency of RhB and caffeine removal (Kuang *et al.* 2013; Guo *et al.* 2020).

Previous studies have demonstrated that the heterogeneous Fenton-like system can be effectively described by pseudo-first- and pseudo-second-order kinetics models (Anchan *et al.* 2019; Guo *et al.* 2020; Hassan *et al.* 2020; Yuan *et al.* 2020). Hence, these models were applied in this study, considering degradation data at various temperatures (25, 35, and 45 °C). The first-order and second-order dynamic fitting curves are presented in Figures 10 and 11, respectively, with detailed kinetic parameters provided in Table 1.

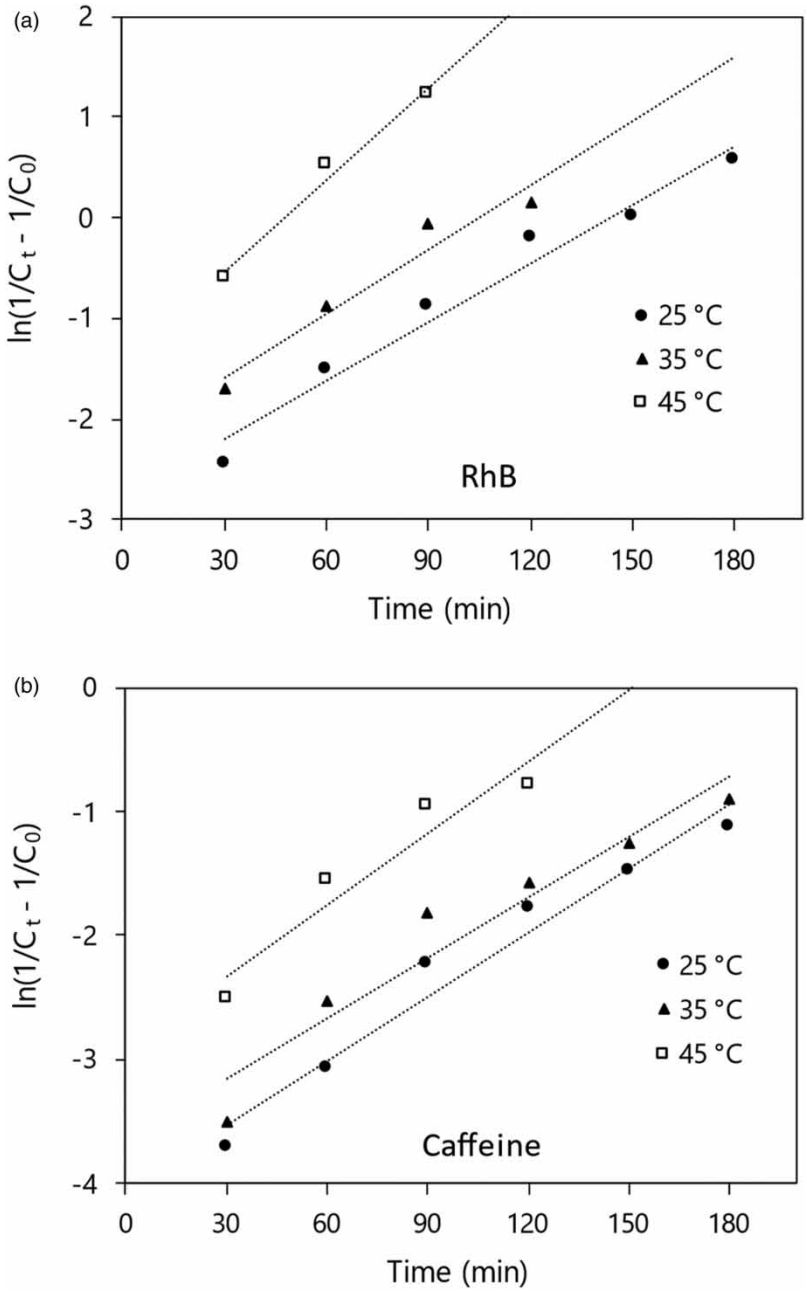

Figure 11 | Pseudo-second-order kinetic model for RhB (a) and caffeine (b) degradation.

Table 1 | Kinetics parameters for RhB and caffeine degradation

	RhB				Caffeine			
	First-order		Second-order		First-order		Second-order	
Temperature (°C)	k_1	R^2	k_2	R^2	k_1	R^2	k_2	R^2
25	0.0191	0.968	0.0194	0.968	0.0114	0.993	0.0173	0.964
35	0.0261	0.920	0.0212	0.954	0.0121	0.976	0.0162	0.929
45	0.0460	0.917	0.0303	0.985	0.0195	0.933	0.0192	0.912

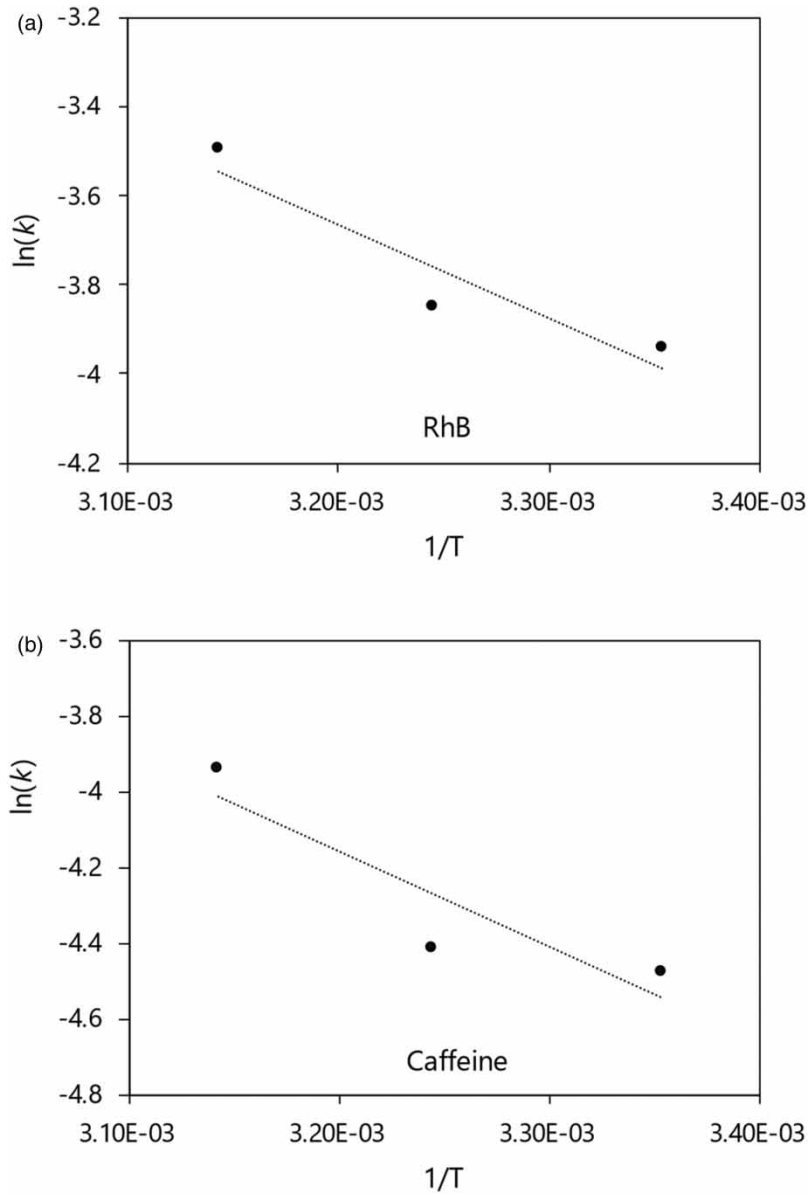

Figure 12 | Linear plot of the Arrhenius equation used for determining the activation energy in the oxidative degradation of RhB and caffeine.

For RhB degradation, the determination coefficients (R^2) for the pseudo-first-order model (0.917–0.968) and the pseudo-second-order model (0.954–0.985) indicated good fits for both models (Table 1), suggesting that RhB degradation involves prompt adsorption and simultaneous oxidation processes. However, the higher R^2 values for the pseudo-second-order

Table 2 | Phytotoxicity studies of RhB, caffeine, and their degraded products after Fenton-like oxidation of RhB and caffeine by FeNPs on *C. sativus*

Parameters studied	Control (distilled water)	RhB solution (20 mg/L)	Degraded product of RhB	Caffeine solution (20 mg/L)	Degraded product of caffeine
Germination (%)	100	100	100	100	100
Radicle (cm)	6.44 ± 1.09	3.86 ± 0.79*	6.50 ± 1.24	6.19 ± 1.01	6.04 ± 0.82
Hypocotyl (cm)	2.68 ± 0.53	1.96 ± 0.54*	2.98 ± 0.93	2.23 ± 0.42	2.50 ± 0.65

Values are mean of three replicates (mean ± standard error).
*Significant differences were observed from the control (seeds germinated in distilled water) using ANOVA with the Tukey–Kramer multiple comparison test ($p < 0.05$).

model imply that the degradation of RhB is predominantly governed by a redox process (Guo *et al.* 2020). Similar conclusions were obtained for the degradation of methylene blue (Anchan *et al.* 2019) and reactive blue 238 (Hassan *et al.* 2020) using the Fenton system with green FeNPs. The reaction rate (k_2) calculated using the pseudo-second-order model at 25, 35, and 45 °C is 0.0194, 0.0212, and 0.0303 L mg^{-1} min^{-1}, respectively.

The fittings for caffeine degradation were also satisfactory for both models. The R^2 values ranged from 0.933 to 0.993 for the pseudo-first-order kinetic model and from 0.912 to 0.964 for the pseudo-second-order kinetic model. Nevertheless, the pseudo-first-order model showed better agreement with the experimental data. The reaction rate (k_1) increased from 0.0114 to 0.0195 with the temperature rising from 25 to 45 °C.

Utilizing the kinetic data, the activation energy (E_a, J mol^{-1}) for the degradation of RhB and caffeine was determined using the Arrhenius equation (Equation (8)):

$$\ln(k) = \ln A - \frac{E_a}{RT} \tag{8}$$

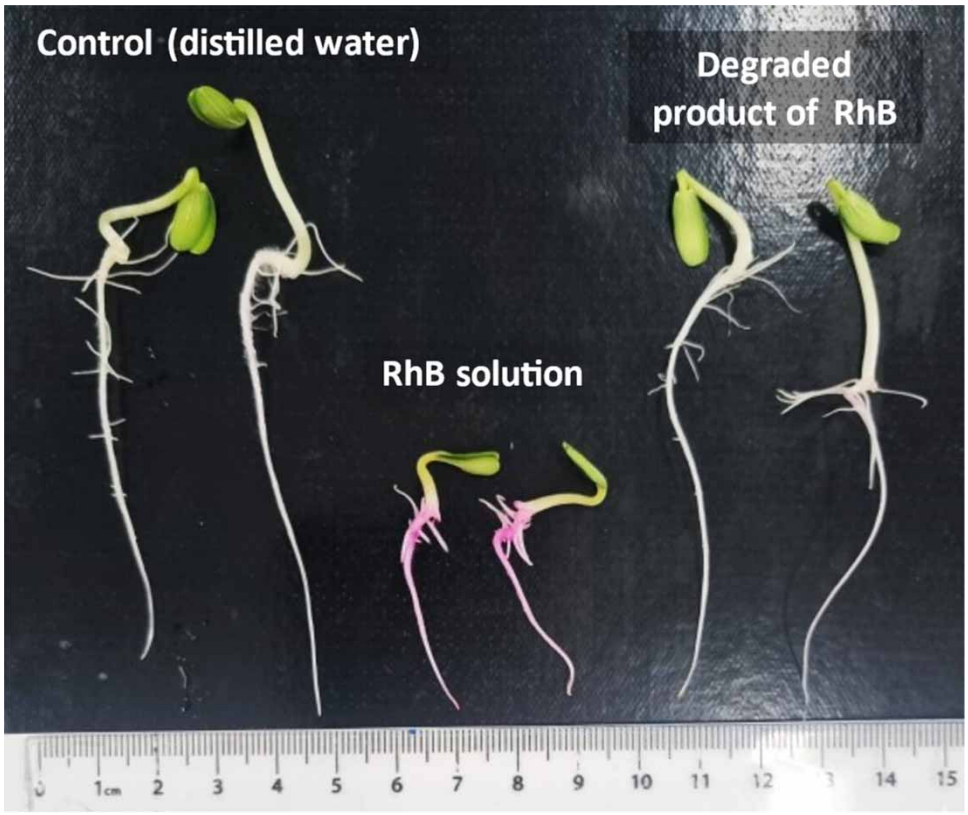

Figure 13 | Appearance of some *C. sativus* seedlings germinated in distilled water, RhB solution, and degraded product of RhB.

where A is the pre-exponential factor, R is the universal gas constant (8.314 J mol^{-1} K^{-1}), and T is the absolute temperature (K). The E_a was calculated by plotting ln(k) versus 1/T (Figure 12).

The E_a for the oxidative degradation of RhB and caffeine was 17.46 and 20.98 kJ mol^{-1}, respectively. Typically, surface-controlled reactions exhibit higher E_a (>29 kJ mol^{-1}) compared to diffusion-controlled reactions (8–21 kJ mol^{-1}) in a solution. The calculated E_a values in this study indicate that the degradation of RhB and caffeine by FeNPs/H_2O_2 is a diffusion-controlled reaction. This conclusion aligns with those reported by Wu *et al.* (2015) and Li *et al.* (2015) who used green FeNPs for degrading malachite green and 2,4-dichlorophenol, respectively.

Phytotoxicity of degradation products from RhB and caffeine

Phytotoxicity tests were conducted with *C. sativus* (cucumber) seeds to examine the potential toxic effects of RhB and caffeine degradation products. The germination of the seeds was not affected by RhB, caffeine, or their degradation products; 100% seed germination was observed (Table 2). However, the development of seedlings was adversely impacted by the RhB solution, leading to a noticeable reduction in growth (Figure 13). Specifically, the average radicle length and hypocotyl length of *C. sativus* were 3.86 and 1.96 cm, respectively, in the presence of the RhB solution. In contrast, when placed in distilled water, the radicle and hypocotyl average lengths increased to 6.44 and 2.68 cm, respectively (Table 2). These differences were statistically significant, considering the use of analysis of variance (ANOVA). When the solution containing the degradation products of RhB was tested, this toxic effect was no longer observed. The lengths of radicle and hypocotyl of 6.50 and 2.98 cm, respectively, clearly indicate the absence of toxicity. In relation to the caffeine solution and its degradation products, no toxic effects were observed on the development of *C. sativus* seedlings. The average lengths of the radicle and hypocotyl for these two solutions did not differ from those obtained for seedlings grown in distilled water. The use of FeNPs demonstrates promising potential for degrading RhB and caffeine, as evidenced by the non-toxic nature of their degradation products.

CONCLUSION

In this study, FeNPs were successfully synthesized using an aqueous extract from the EB. The synthesis method employed is characterized by its simplicity, efficiency, and sustainability. The characterization of FeNPs revealed their spherical morphology with an average diameter of 419.2 nm. The nanoparticles exhibited an amorphous nature, as observed through XRD analysis. FTIR analysis confirmed the role of phytochemicals in the baru endocarp extract, capping, and stabilizing the nanoparticles. The FeNPs demonstrated excellent catalytic activity, achieving removal efficiencies of 99.14% for RhB and 92.01% for caffeine. This was observed at an initial solution pH of 3.0, after 180 min, using 1.0 g L^{-1} of FeNPs, 1% H_2O_2, and a temperature of 45 °C. Effective degradation of RhB and caffeine was also noted in a higher pH range (4–6), highlighting significant practical applications. The catalytic reaction kinetics were modeled as pseudo-first-order for caffeine and pseudo-second-order for RhB. The activation energy for the degradation of RhB and caffeine was calculated as 17.46 and 20.98 kJ mol^{-1}, respectively, indicating that the degradation of these organic compounds by FeNPs/H_2O_2 is a diffusion-controlled reaction. Studies on the phytotoxicity of the degraded products of RhB and caffeine with *C. sativus* confirmed their non-toxic nature, supporting the feasibility of employing FeNPs as an environmentally friendly solution for water treatment. This approach offers a sustainable method for pollutant remediation in aquatic environments.

DATA AVAILABILITY STATEMENT

All relevant data are included in the paper or its Supplementary Information.

CONFLICT OF INTEREST

The authors declare there is no conflict.

REFERENCES

Alabdallah, N. M., Hasan, M. M., Hammami, I., Alghamdi, A. I., Alshehri, D. & Alatawi, H. A. 2021 Green synthesized metal oxide nanoparticles mediate growth regulation and physiology of crop plants under drought stress. *Plants* **10** (8), 1–13. https://doi.org/10.3390/plants10081730.

Anchan, S., Pai, S., Sridevi, H., Varadavenkatesan, T., Vinayagam, R. & Selvaraj, R. 2019 Biogenic synthesis of ferric oxide nanoparticles using the leaf extract of *Peltophorum pterocarpum* and their catalytic dye degradation potential. *Biocatalysis and Agricultural Biotechnology* **20**, 1–10. https://doi.org/10.1016/j.bcab.2019.101251.

Aneke, F. & Adu, J. 2023 Adsorption of heavy metals from contaminated water using leachate modular tower. *Civil Engineering Journal* **9** (6), 1522–1541. http://dx.doi.org/10.28991/CEJ-2023-09-06-017.

Babuponnusami, A. & Muthukumar, K. 2012 Removal of phenol by heterogeneous photo electro Fenton-like process using nano-zero valent iron. *Separation and Purification Technology* **98**, 130–135. https://doi.org/10.1016/j.seppur.2012.04.034.

Bachmann, S. A. L., Calvete, T. & Féris, L. A. 2021 Caffeine removal from aqueous media by adsorption: An overview of adsorbents evolution and the kinetic, equilibrium and thermodynamic studies. *Science of the Total Environment* **767**, 1–13. https://doi.org/10.1016/j.scitotenv.2020.144229.

Barizão, A. C., Silva, M. F., Andrade, M., Brito, F. C., Gomes, R. G. & Bergamasco, R. 2020 Green synthesis of iron oxide nanoparticles for tartrazine and Bordeaux red dye removal. *Journal of Environmental Chemical Engineering* **8** (1), 1–10. https://doi.org/10.1016/j.jece.2019.103618.

Bharathi, D., Preethi, S., Abarna, K., Nithyasri, M., Kishore, P. & Deepika, K. 2020 Bio-inspired synthesis of flower shaped iron oxide nanoparticles (FeONPs) using phytochemicals of *Solanum lycopersicum* leaf extract for biomedical applications. *Biocatalysis and Agricultural Biotechnology* **27**, 1–8. https://doi.org/10.1016/j.bcab.2020.101698.

Briton, B. G. H., Duclaux, L., Richardson, Y., Yao, K. B., Reinert, L. & Soneda, Y. 2019 Effectiveness of the dispersion of iron nanoparticles within micropores and mesopores of activated carbon for Rhodamine B removal in wastewater by the heterogeneous Fenton process. *Applied Water Science* **9**, 1–14. https://doi.org/10.1007/s13201-019-1047-0.

Cruz, D., Almeida, A., Calisto, V., Esteves, V. I., Schneider, R. J., Wrona, F. J., Soares, A. M. V. M., Figueira, E. & Freitas, R. C. 2016 Caffeine impacts in the clam Ruditapes philippinarum: Alterations on energy reserves, metabolic activity and oxidative stress biomarkers. *Chemosphere* **160**, 95–103. https://doi.org/10.1016/j.chemosphere.2016.06.06.

Demirezen, D. A., Yiliz, Y. Ş. & Ylmaz, D. D. 2019 Green synthesis and characterization of iron oxide nanoparticles using *Ficus carica* (common fig) dried fruit extract. *Journal of Bioscience and Bioengineering* **127** (2), 241–245. https://doi.org/10.1016/j.jbiosc.2018.07.024.

Dhahir, S. A., Al-Saade, K. & Al-Jobouri, S. 2014 Degradation studies of Rhodamine B in the presence of UV/H_2O_2/Fe^{2+}. *International Journal of Technical Research and Applications* **2** (6), 123–127.

Fahmy, H. M., Mohamed, F. M., Marzouq, M. H., Mustafa, A. B. E. D., Alsoudi, A. M., Ali, O. A., Mohamed, M. A. & Mahmoud, F. A. 2018 Review of green methods of iron nanoparticles synthesis and applications. *BioNanoScience* **8** (2), 491–503. https://doi.org/10.1007/s12668-018-0516-5.

Golin, R., Barbosa, A. G., Lopes, V. C. P., Caixeta, D. S., de Menezes Filho, F. C. M., Dall'oglio, E. L., de Vasconcelos, L. G. & de Morais, E. B. 2022 Decolorization of Rhodamine B by Fenton reaction using iron nanoparticles supported in Brazil nutshell biomass. *Revista Materia* **27** (3), 1–11. https://doi.org/10.1590/1517-7076-RMAT-2022-0039.

Guo, B., Xu, T., Zhang, L. & Li, S. 2020 A heterogeneous fenton-like system with green iron nanoparticles for the removal of bisphenol A: Performance, kinetics and transformation mechanism. *Journal of Environmental Management* **272**, 1–9. https://doi.org/10.1016/j.jenvman.2020.111047.

Hassan, A. K., Al-Kindi, G. Y. & Ghanim, D. 2020 Green synthesis of bentonite-supported iron nanoparticles as a heterogeneous Fenton-like catalyst: Kinetics of decolorization of reactive blue 238 dye. *Water Science and Engineering* **13** (4), 286–298. https://doi.org/10.1016/j.wse.2020.12.001.

Haydar, M. D., Ghosh, S. & Mandal, P. 2022 Application of iron oxide nanoparticles as micronutrient fertilizer in mulberry propagation. *Journal of Plant Growth Regulation* **41**, 1726–1746. https://doi.org/10.1007/s00344-021-10413-3.

Ismail, W. N. W., Syah, M. I. A. I., Muhet, N. H. A., Bakar, N. H. A., Yusop, H. M. & Samah, N. A. 2022 Adsorption behavior of heavy metal ions by hybrid Inulin-TEOS for water treatment. *Civil Engineering Journal* **8** (9), 1787–1798. http://dx.doi.org/10.28991/CEJ-2022-08-09-03.

Irshad, R., Tahir, K., Li, B., Ahmad, A., Siddiqui, A. R. & Nazir, S. 2017 Antibacterial activity of biochemically capped iron oxide nanoparticles: A view towards green chemistry. *Journal of Photochemistry and Photobiology B: Biology* **170**, 241–246. https://doi.org/10.1016/j.jphotobiol.2017.04.020.

Jadoun, S., Arif, R., Jangid, N. K. & Meena, R. K. 2021 Green synthesis of nanoparticles using plant extracts: A review. *Environmental Chemistry Letters* **19** (1), 355–374. https://doi.org/10.1007/s10311-020-01074-x.

Jain, R., Mendiratta, S., Kumar, L. & Srivastava, A. 2021 Green synthesis of iron nanoparticles using *Artocarpus heterophyllus* peel extract and their application as a heterogeneous Fenton-like catalyst for the degradation of Fuchsin Basic dye. *Current Research in Green and Sustainable Chemistry* **4**, 1–8. https://doi.org/10.1016/j.crgsc.2021.100086.

Jijie, R., Mihalache, G., Balmus, I. M., Strungaru, S.-A., Baltag, E. S., Ciobica, A., Nicoara, M. & Faggio, C. 2021 Zebrafish as a screening model to study the single and joint effects of antibiotics. *Pharmaceuticals* **14**, 1–26. https://doi.org/10.3390/ph14060578.

Khoshkalam, E., Fotovat, A., Halajnia, A., Kazemian, H. & Eshghi, H. 2023 Nitrate adsorption using green iron oxide nanoparticles synthesized by *Eucalyptus* leaf extracts: Kinetics and effects of pH, KCl salt, and anions competition. *Journal of Molecular Liquids* **375**, 1–11. https://doi.org/10.1016/j.molliq.2023.121366.

Korekar, G., Kumar, A. & Ugale, C. 2020 Occurrence, fate, persistence and remediation of caffeine: A review. *Environmental Science and Pollution Research* **27** (28), 34715–34733. https://doi.org/10.1007/s11356-019-06998-8.

Kuang, Y., Wang, Q., Chen, Z., Megharaj, M. & Naidu, R. 2013 Heterogeneous Fenton-like oxidation of monochlorobenzene using green synthesis of iron nanoparticles. *Journal of Colloid and Interface Science* **410**, 67–73. https://doi.org/10.1016/j.jcis.2013.08.020.

Li, R., Gao, Y., Jin, X., Chen, Z., Megharaj, M. & Naidu, R. 2015 Fenton-like oxidation of 2,4-DCP in aqueous solution using iron-based nanoparticles as the heterogeneous catalyst. *Journal of Colloid and Interface Science* **438**, 87–93. https://doi.org/10.1016/j.jcis.2014.09.082.

Li, S., Wen, J., He, B., Wang, J., Hu, X. & Liu, J. 2020 Occurrence of caffeine in the freshwater environment: Implications for ecopharmacovigilance. *Environmental Pollution* **263**, 1–14. https://doi.org/10.1016/j.envpol.2020.114371.

Lourenço, I. M., Pieretti, J. C., Nascimento, M. H. M., Lombello, C. B. & Seabra, A. B. 2019 Eco-friendly synthesis of iron nanoparticles by green tea extract and cytotoxicity effects on tumoral and non-tumoral cell lines. *Energy, Ecology and Environment* **4** (6), 261–270. https://doi.org/10.1007/s40974-019-00134-5.

Madubuonu, N., Aisida, S. O., Ali, A., Ahmad, I., Zhao, T. K., Botha, S., Maaza, M. & Ezema, F. I. 2019 Biosynthesis of iron oxide nanoparticles via a composite of *Psidium guavaja-Moringa oleifera* and their antibacterial and photocatalytic study. *Journal of Photochemistry and Photobiology B: Biology* **199**, 1–9. https://doi.org/10.1016/j.jphotobiol.2019.111601.

Muñoz-Peñuela, M., Lo Nostro, F. L., Gomes, A. D. O., Tolussi, C. E., Branco, G. S., Pinheiro, J. P. S., Godoi, F. G. A. & Moreira, R. G. 2021 Diclofenac and caffeine inhibit hepatic antioxidant enzymes in the freshwater fish *Astyanax altiparanae* (Teleostei: Characiformes). *Comparative Biochemistry and Physiology Part C* **240**, 1–8. https://doi.org/10.1016/j.cbpc.2020.108910.

Narayanan, M., Divya, S., Natarajan, D., Senthil-Nathan, S., Kandasamy, S., Chinnathambi, A., Alahmadi, T. A. & Pugazhendhi, A. 2021 Green synthesis of silver nanoparticles from aqueous extract of *Ctenolepis garcini* L. and assess their possible biological applications. *Process Biochemistry* **107**, 91–99. https://doi.org/10.1016/j.procbio.2021.05.008.

Niedack, L. O. C., Souza, L. G. S., Alves, L. E. O. & Damiani, C. R. 2021 Baru (*Dipteryx alata* Vogel), a woody species characteristic of Cerrado and its phytoremediation potential. *Environmental Science and Pollution Research* **28**, 57798–57806. https://doi.org/10.1007/s11356-021-14708-6.

Ningthoujam, R., Sahoo, B., Ghosh, P., Shivani, A., Ganguli, P. & Chaudhuri, S. 2023 Green production of zero-valent iron nanoparticles using pomegranate peel extracts and its use in lindane degradation. *Nanotechnology for Environmental Engineering* **8** (2), 581–589. https://doi.org/10.1007/s41204-023-00313-0.

Oliveira, T. D., Martini, W. S., Santos, M. D. R., Matos, M. A. C. & Rocha, L. L. 2015 Caffeine oxidation in water by fenton and fenton-like processes: Effects of inorganic anions and ecotoxicological evaluation on aquatic organisms. *Journal of the Brazilian Chemical Society* **26** (1), 178–184. https://doi.org/10.5935/0103-5053.20140237.

Osuoha, J. O., Anyanwu, B. O., Ejileugha, C., 2023 Pharmaceuticals, personal care products as emerging contaminants: Need for combined treatment strategy. *Journal of Hazardous Materials Advances* **9**, 100206. https://doi.org/10.1016/j.hazadv.2022.100206.Pai, S., Kini, S. M., Narasimhan, M. K., Pugazhendhi, A. & Selvaraj, R. 2021 Structural characterization and adsorptive ability of green synthesized Fe_3O_4 nanoparticles to remove Acid blue 113 dye. *Surfaces and Interfaces* **23**, 1–9. https://doi.org/10.1016/j.surfin.2021.100947.

Priya, N., Kaur, K. & Sidhu, A. K. 2021 Green synthesis: An eco-friendly route for the synthesis of iron oxide nanoparticles. *Frontiers in Nanotechnology* **3**, 1–16. https://doi.org/10.3389/fnano.2021.655062.

Rambo, M. K. D., Nemet, Y. K. S., Júnior, C. C. S., Mendes Pedroza, M. & Rambo, M. C. D. 2021 Comparative study of the products from the pyrolysis of raw and hydrolyzed baru wastes. *Biomass Conversion and Biorefinery* **11**, 1943–1953. https://doi.org/10.1007/s13399-019-00585-0.

Rani, C. N. 2022 Photocatalytic degradation of caffeine in a slurry reactor with intermittent UV irradiation: Optimization and response surface modelling. *Water Practice and Technology* **17** (1), 517–528. https://doi.org/10.2166/wpt.2021.130.

Ríos, A. L. M., Gutierrez-Suarez, K., Carmona, Z., Ramos, C. G. & Oliveira, L. F. S. 2022 Pharmaceuticals as emerging pollutants: Case naproxen an overview. *Chemosphere* **291**, 132822. https://doi.org/10.1016/j.chemosphere.2021.132822.

Rocker, C., Caetano, J., Gonçalves Júnior, A. C., Mees, J. B. R. & Dragunski, D. C. 2019 Biosorption of Cr(III) ions from synthetic aqueous solutions and tannery effluent using the macrophyte *Pistia stratiotes*. *Engenharia Sanitaria e Ambiental* **24** (2), 335–346. https://doi.org/10.1590/S1413-41522019159636.

Rolim, W. R., Pelegrino, M. T., de Araújo Lima, B., Ferraz, L. S., Costa, F. N., Bernardes, J. S., Rodigues, T., Brocchi, M. & Seabra, A. B. 2019 Green tea extract mediated biogenic synthesis of silver nanoparticles: Characterization, cytotoxicity evaluation and antibacterial activity. *Applied Surface Science* **463**, 66–74. https://doi.org/10.1016/j.apsusc.2018.08.203.

Rusevova, K., Kopinke, F.-D. & Georgi, A. 2012 Nano-sized magnetic iron oxides as catalysts for heterogeneous Fenton-like reactions – Influence of Fe(II)/Fe(III) ratio on catalytic performance. *Journal of Hazardous Materials* **241–242**, 433–440. https://doi.org/10.1016/j.jhazmat.2012.09.068.

Selvaraj, R., Pai, S., Vinayagam, R., Varadavenkatesan, T., Kumar, P. S., Duc, P. A. & Rangasamy, G. 2022 A recent update on green synthesized iron and iron oxide nanoparticles for environmental applications. *Chemosphere* **308**, 1–12. https://doi.org/10.1016/j.chemosphere.2022.136331.

Suppiah, D. D., Julkapli, N. M., Sagadevan, S. & Johan, M. R. 2023 Eco-friendly green synthesis approach and evaluation of environmental and biological applications of iron oxide nanoparticles. *Inorganic Chemistry Communications* **152**, 1–12. https://doi.org/10.1016/j.inoche.2023.110700.

Talib, A. & Randhir, T. O. 2017 Managing emerging contaminants in watersheds: Need for comprehensive, systems-based strategies. *Sustainability of Water Quality and Ecology* **9–10**, 1–8. https://doi.org/10.1016/j.swaqe.2016.05.002.

Ting, A. S. Y. & Chin, J. E. 2020 Biogenic synthesis of iron nanoparticles from apple peel extracts for decolorization of Malachite green dye. *Water, Air, and Soil Pollution* **231** (6), 1–10. https://doi.org/10.1007/s11270-020-04658-z.

Valdez-Carrillo, M., Abrell, L., Ramírez-Hernández, J., Reyes-López, J. A. & Carreón-Diazconti, C. 2020 Pharmaceuticals as emerging contaminants in the aquatic environment of Latin America: A review. *Environmental Science and Pollution Research* **27**, 44863–44891. https://doi.org/10.1007/s11356-020-10842-9.

Wang, C., Cao, Y. & Wang, H. 2019 Copper-based catalyst from waste printed circuit boards for effective Fenton-like discoloration of Rhodamine B at neutral pH. *Chemosphere* **230**, 278–285. https://doi.org/10.1016/j.chemosphere.2019.05.068.

Wu, Y., Zeng, S., Wang, F., Megharaj, M., Naidu, R. & Chen, Z. 2015 Heterogeneous Fenton-like oxidation of malachite green by iron-based nanoparticles synthesized by tea extract as a catalyst. *Separation and Purification Technology* **154**, 161–167. https://doi.org/10.1016/j.seppur.2015.09.022.

Xiao, Z., Yuan, M., Yang, B., Liu, Z., Huang, J. & Sun, D. 2016 Plant-mediated synthesis of highly active iron nanoparticles for Cr(VI) removal: Investigation of the leading biomolecules. *Chemosphere* **150**, 357–364. https://doi.org/10.1016/j.chemosphere.2016.02.056.

Yuan, M., Fu, X., Yu, J., Xu, Y., Huang, J., Li, Q. & Sun, D. 2020 Green synthesized iron nanoparticles as highly efficient Fenton-like catalyst for degradation of dyes. *Chemosphere* **261**, 1–8. https://doi.org/10.1016/j.chemosphere.2020.127618.

First received 14 November 2023; accepted in revised form 14 March 2024. Available online 25 March 2024